Received: 22 February 2021 | Revised: 6 July 2021 | Accepted: 23 July 2021

DOI: 10.1111/cbdd.13939

RESEARCH ARTICLE

WILEY

Design, synthesis, and biological evaluation of benzo[b]thiophene 1,1-dioxide derivatives as potent STAT3 inhibitors

Wen-Zhen Li[1]* | Hui-Zhi Xi[1]* | Yi-Jie Wang[1]* | Hong-Bo Ma[2] | Zhi-Qiang Cheng[3] | Yu Yang[1] | Meng-Ling Wu[1] | Ting-Mei Liu[1] | Wen Yang[1] | Qin Wang[1] | Meng-Ya Liao[4] | Yong Xia[1] | Yi-Wen Zhang[1]

[1]Cancer Center, West China Hospital, Sichuan University, Chengdu, China

[2]West China School of Pharmacy, Sichuan University, Chengdu, China

[3]Department of Pharmacology and Molecular Sciences, Johns Hopkins University School of Medicine, Baltimore, MD, USA

[4]Center of Gerontology and Geriatrics, West China Hospital, Sichuan University, Chengdu, China

Correspondence
Yi-Wen Zhang and Yong Xia, Cancer Center, West China Hospital, Sichuan University, Chengdu, China.
Email: yiwenzhang@scu.edu.cn; scuxiayong@163.com

Meng-Ya Liao, Center of Gerontology and Geriatrics, West China Hospital, Sichuan University, Chengdu, China.
Email: 507162040@qq.com

Funding information
Support Program of Science & Technology Department of Sichuan Provincial, Grant/Award Number: 2021YFH0173

Abstract

As a member of the signal transducer and activator of transcription (STAT) family, STAT3 plays a critical role in several biological pathways such as cell proliferation, migration, survival, and differentiation. Due to abnormal continuous activation in tumors, inhibition of STAT3 has emerged as an attractive approach for the treatment of various cancer cells. Herein, we report a series of novel STAT3 inhibitors based on benzo[b]thiophene 1,1-dioxide scaffold and evaluated their anticancer potency. Among them, compound **8b** exhibited the best activity against cancer cells. Compound **8b** induced apoptosis and blocked the cell cycle. Meanwhile, **8b** reduced intracellular ROS content and caused the loss of mitochondrial membrane potential. Further research revealed that **8b** significantly blocked STAT3 phosphorylation and STAT3-dependent dual-luciferase reporter gene experiments showed that compound **8b** has a marked inhibition of STAT3-mediated Firefly luciferase activity. Molecular modeling studies revealed compound **8b** occupied the pocket well with the SH2 domain in a favorable conformation.

KEYWORDS

apoptosis, cell cycle, inhibitors, mitochondrial membrane potential, ROS, STAT3, tumors

1 | INTRODUCTION

Signal transducer and activator of transcription (STAT) family consist of seven members, STAT1, 2, 3, 4, 5α, 5β, 6 (Darnell, 1997). Among them, STAT1, STAT3, and STAT5 are highly associated with human tumorigenesis and development due to their frequent hyperactivation (Benekli et al., 2009). In normal cells, STAT3 responds to the stimulation of various extracellular signaling factors and then transmits them through phosphorylation of the tyrosine kinase site (Tyr705) in the SH2 domain. Once in the nucleus, STAT3 binds to DNA and subsequently activates transcription and translation, thus performing various physiological functions (Furtek et al., 2016; Ren et al., 2015; Yamamoto et al., 2002). However, according to previous research, STAT3 is involved in the process of growth, proliferation, angiogenesis, and invasion of tumor cells (Bromberg & Chen, 2001). Abnormally high expression

*These authors contribute equally.

and persistent activation of STAT3 have been observed in many human solid and hematological tumors, such as ovarian cancer (Huang et al., 2000), pancreatic cancer (Sun et al., 2014), prostate cancer (Liao & Nevalainen, 2011), head and neck cancer (Cohen-Kaplan et al., 2012), breast cancer (Barash, 2012), leukemia (Casetti et al., 2013), and non-small cell lung carcinoma (Sanchez-Ceja et al., 2006). In general, hyperactivation of STAT3 upregulates the expression of many downstream transcriptional genes, including the anti-apoptotic proteins Bcl-xL and the Bcl-2, proliferation-related proteins cyclin D1 and c-Myc, MMP-2, and MMP-9, which are associated with migration and invasion-related proteins, and the pro-angiogenesis factor VEGF (Germain & Frank, 2007; Yu et al., 2009). More importantly, the expression of above oncogenes is not the only way leading to cancer. Activation of STAT3 also promotes the occurrence of cancer through immunosuppression in immune cells (Wang et al., 2018).

During the past decades, the development of STAT3 inhibitors has been a popular strategy for the treatment of various tumors. Although plenty of STAT3 inhibitors has been reported, there are still no FDA-approved drugs on the market. STAT3 contains 6 domains, including N-terminated conserved domain, coiled-coil domain, DNA-binding site domain, linker domain, SH2 domain, and C-terminated activated domain (Furtek et al., 2016). Among them, the key SH2 domain is responsible for STAT3 phosphorylation and homodimerization. The process of phosphorylation and homodimerization could be disrupted by small molecules therefore providing a feasible way for STAT3 inhibitor drug discovery. (Furtek et al., 2016).

Stattic is the first small molecule inhibitor targeting the SH2 domain (Schust et al., 2006). Based on Stattic, several derivatives were synthesized, such as HJC0416, HJC0123, and E28 (Chen et al., 2014; Chen et al., 2013; Ji et al., 2015). Besides, STA-21, LLL-3, LLL-12, and BBI608 which share common moiety were also representative inhibitors binding to SH2 domain(Bhasin et al., 2008; Chen et al., 2007; Lin et al., 2010; Song et al., 2005; Zhang et al., 2016)

Previous works have indicated that pY and pY-X cavities in the SH2 domain are critical for inhibitor activity and selectivity (Maritano et al., 2004; Park & Li, 2011). We found that Stattic only occupied the pY-X cavity, leaving the pY cavity empty (Figure S1). We hired a virtual screening program to find the appropriate fragment targeting the pY cavity. In accordance with the results, ligustrazine, reported to treat tumors through ROS mediation (Han et al., 2015), was induced into pY cavity to obtain superior activity and selectivity. Finally, 28 compounds were synthesized, among them **8b** was proved the best compound possessing exceptional property as a potential candidate.

2 | MATERIALS AND METHOD

All chemical reagents and solvents were bought from Energy Chemical or Chron Chemicals. Thin-layer chromatography (TLC) was inducted to monitor reaction process, and column chromatography was carried out on 200–300 mesh silica gel. UV light was used to visualize products. All compounds were characterized by ^{1}H-NMR (401 MHz, Bruker Avance400) and ^{13}C-NMR (101 MHz, Bruker Avance400). TMS was used as internal standard. Q-TOF Premier mass spectrometer (Micromass) was applied to measure mass spectrum.

2.1 | Chemicals

We synthesized these compounds according to the synthetic route described in Scheme 1. In short, 2-fluorobenzaldehyde and its derivatives were used as the starting materials and reacted with methyl thioglycolate in DMF to obtain **2a–2m**. Subsequently, **2a–2m** removed the methyl ester in NH_4Cl/MeOH solvent leading to **3a–3m**. Various amino derivatives reacted with **3a–3m** to obtain **4a–4o**. Then, **4a–4o** were oxidized by 3-chloroperoxybenzoic acid in DCM, giving **5a–5o**. The boc protecting group was subsequently removed by trifluoroacetic acid to form **6a–6o**. **6a–6o** were coupled with 3,5,6-trimethylpyrazine-2-carbo xylic acid to get **7a–7o**. **8a–8m** were obtained through the alkylation of **6a–6m**. 3,5,6-Trimethylpyrazine-2-carboxyl ic acid and 2-(bromomethyl)-3,5,6-trimethylpyrazine were prepared from tetramethylpyrazine (Ligustrazine). Details can be found in the reported method (Chen et al., 2015; Wang et al., 2019).

2.2 | Cell culture and materials

All cell lines including human colorectal cancer cell line HCT116, human breast adenocarcinoma cell lines MCF-7 and MDA-MB-231, human liver hepatocellular carcinoma HepG2 were obtained from American Type Culture Collection (ATCC). The cells were cultured in DMEM containing 10% fetal bovine serum (v/v) and maintained at 37℃ under 5% CO_2.

2.3 | Cell antiproliferation assays

The antiproliferation activities of synthesized compounds were determined in the HCT116 cells, MCF-7 cells, MDA-MB-231 cells, and HepG2 cells. Cells (5×10^7/L) were seeded in 96-well plates and allowed to incubate for 24 hr. Then, cells were treated with compounds

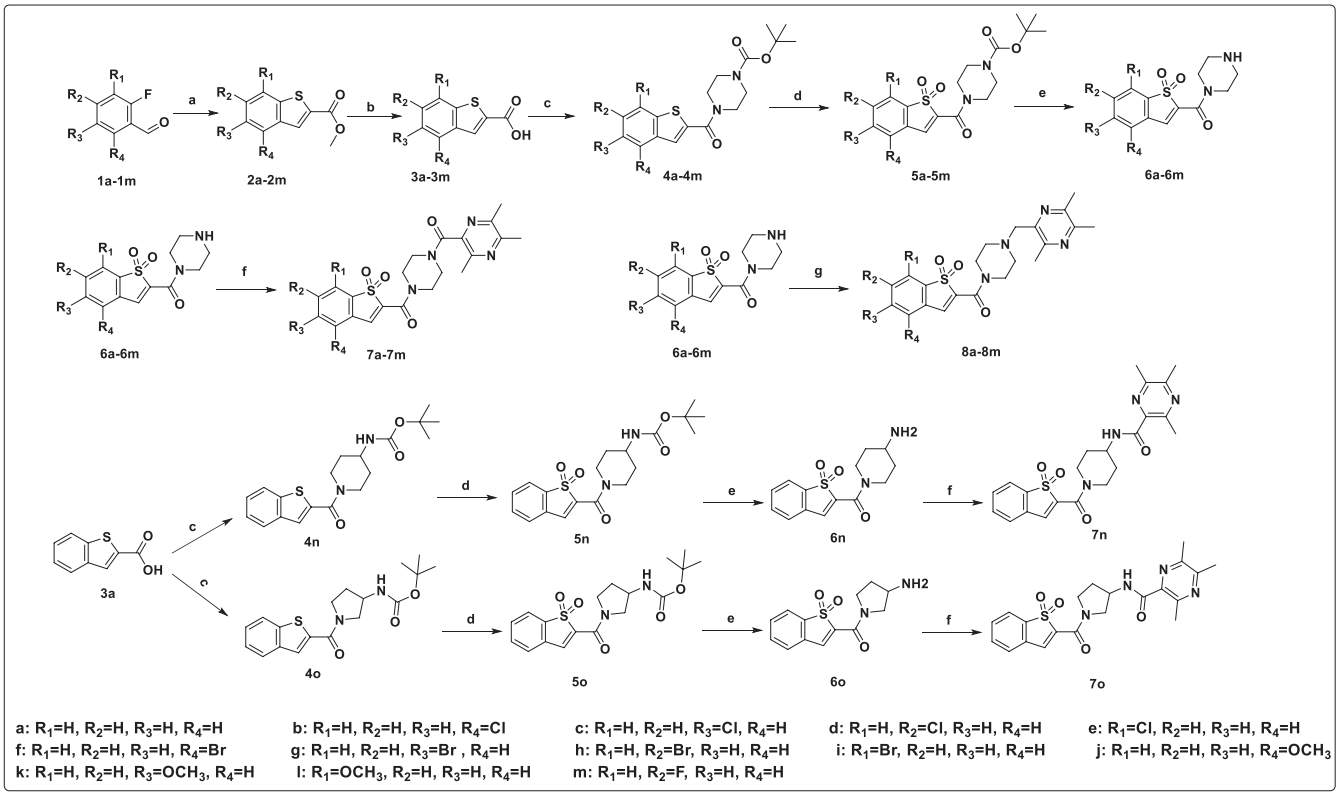

SCHEME 1 (a) $HSCH_2COOCH_3$, DMF, 60°C, 15 hr, 72%-94%. (b) THF, H_2O, LiOH, HCl, 98%–100%. (c) HATU, DIEA, DMF, rt, overnight, 95%–100%. (d) *m*-CPBA, DCM, 3 hr, 45°C, 45%–60%. (e) DCM, TFA (98%), rt, 3hr. (f) HATU, DIEA, 3,5,6-trimethylpyrazine-2-carboxylic acid, DCM, rt, 40%–60%. (g) KI, CH_3CN, 2-(bromomethyl)-3,5,6-trimethylpyrazine, reflux, 1.5 hr, 35%–47%

(0–20 μM) for 72 hr. After that, 10 μl of MTT reagent (5 mg/ml) was added per well followed by extra 2- to 4-hr incubation. Formazan precipitates were dissolved in 150 μl of 100% DMSO, and absorbance was determined at 570 nm by a microplate reader 3550-UV (Thermo Fisher Scientific).

2.4 | Flow cytometry analysis of apoptotic cells and cell cycle

Apoptosis assays were determined in HCT116, MCF-7 cells, MDA-MB-231 cells, and HepG2 cells. Cells (5×10^7/L) were seeded in six-well plates and treated with compound **8b** (0, 2.5, 5, 10 μM) for 48 hr. Then, the cells were harvested and washed with PBS. The apoptosis-induced effect was checked by Annexin V/FITC Apoptosis Detection Kit I (Keygen Tec).

Cell cycle assays were performed in HCT116, MCF-7 cells, and HepG2 cells. Cells (5×10^7/L) were seeded in six-well plates and treated with compound **8b** (0, 2.5, 5, 10 μM) for 48 hr. After collection and PBS washing, the cells were fixed by 70% ethanol at −20°C for 8 hr. The cells were harvested and washed with PBS and resuspended in propidium iodide (PI)/RNase-free staining solution. After, the samples were analyzed by flow cytometer (ACEA Biosciences Inc).

2.5 | ROS detections

MCF-7 cells and HepG2 cells were exploited to detect intramolecular ROS level. Cells (5×10^7/L) were cultured in six-well plates and treated with compound **8b** or vehicle. After treatment, the growth media was replaced with serum-free medium containing DCF-DA (10 μM). The cells were harvested and washed with PBS. The ROS level was measured by flow cytometer (ACEA Biosciences Inc).

2.6 | Mitochondrial membrane potential detections

MCF-7 cells and HepG2 cells were used to detect mitochondrial membrane potential. Cells (5×10^7/L) were cultured in six-well plates and treated with compound **8b** or DMSO vehicle. After treatment, cells were incubated with DMEM containing Rh123 (5 μg/ml) for 30 min. The cells were harvested and washed with PBS. The ΔΨm was measured by flow cytometer (ACEA Biosciences Inc).

2.7 | Western Blotting assays

Western Blotting assay was performed in HepG2 cells. The cells (5×10^7/L) were cultured in six-well plates and treated with compound **8b** (1.5, 2.5, 5 μM) or vehicle for 24 hr. Then, the cells were collected and washed by ice-cold PBS and lysis buffer (50 mM Tris–HCl, pH 7.4, 150 mM NaCl, 0.25% deoxycholic acid, 1% NP-40, 1 mM EDTA, and protease inhibitors). Lysates were collected through centrifugation (13, 400 *g*, 10 min, 4℃). An aliquot of samples (30 μg) was subjected to 10% SDS-PAGE and subsequently transferred onto PVDF membranes, blocked by non-fat milk for 1 hr, and blotted with primary antibodies specific for STAT3, p-STAT3, cleaved caspase 3, caspase 3, Bax, Bcl-2, E-cadherin, vimentin cylin B, p-CDC2, γH2AX, p53, and GAPDH at 4℃ for 8 hr. After incubating with corresponding secondary antibodies, bound immuno-complexes were visualized using ELC.

2.8 | STAT3 dual-luciferase reporter assays

HepG2 cells were cultured in 24-well plates (2×10^5 cells/well). After 24 hr of culture, the cells were transiently transfected with pLuc-TK/STAT3 (0.2 mg) and pRL-TK (0.04 mg). 24 hr later, the cells were treated compound **8b** for 48 hr. Then, the cells were washed and lysed according to the protocol. Luciferase activity was measured using a multifunctional enzyme marker (Bio-Rad).

2.9 | Molecular docking study

The crystal structure of STAT3 in complex with DNA was obtained from Protein Data Bank (PDB 1BG1); Schrödinger 10.1 was used to predict the binding modes of **8b**. All docking programs were run with default settings.

3 | RESULT AND DISCUSSION

3.1 | Chemistry

3.1.1 | General procedures for preparation of 2a-2m

To a solution of **1(a-m)** (1 mmol, 1.0 eq) in 10 ml DMF, methyl thioglycolate (1.1 mmol, 2.0 eq) and anhydrous potassium carbonate 1 (2 mmol, 2.0 eq) were added; the reaction were carried out at 60℃ for 8 hr. The reaction was monitored by TLC. After completion, DMF was removed by rotary evaporation under reduced pressure, residues were dissolved in ethyl acetate (30 ml) and washed with saturated brine (10 ml × 3), the organic layer was collected, dried by anhydrous sodium sulfate, purified by silica gel column, and concentrated under reduced pressure. Yield 72%–94%. White solid. **2a**: ^{1}H NMR (401 MHz, $CDCl_3$) δ 8.04 (s, 1H), 7.85 (dd, J = 7.3, 5.8 Hz, 2H), 7.41 (m, 2H), 3.93 (s, 3H).

3.1.2 | General procedures for preparation of 3a-3m

MeOH (10 ml) and water (10 ml) were added to the round-bottom flask which contained **3(a-m)** (1 mmol, 1.0 eq); then, LiOH (3 mmol, 3.0 eq) solid was added; mixture solution was stirred overnight at room temperature. Upon completion, adjusting the pH of the solution to 3 with dilute hydrochloric acid (1 N). The solution was extracted by ethyl acetate (15 ml × 2), collecting the organic phase and concentrating under reduced pressure. Yield 100%. White solid. **3a**: ^{1}H NMR (401 MHz, DMSO-d_6):13.43 (s, 3H), δ 8.54 (s, 1H), 7.82 (dd, J = 7.3, 5.8 Hz, 2H), 7.46 (m, 2H).

3.1.3 | General procedures for preparation of 4a-4o

A mixture of **3(a-m)** (1.0 mmol, 1.0 eq), HATU (1.50 mmol, 1.5 eq), DIEA (4.0 mmol, 4.0 eq) were stirred in anhydrous DMF (20 ml) for 15 min at room temperature; amino (1.0 mmol, 1.1 eq) was added. Reaction was stirred overnight at room temperature. Upon completion, DMF was removed by rotary evaporation under reduced pressure; the residues were dissolved in ethyl acetate (30 ml) and washed with saturated brine (10 ml × 3), collecting the organic layer and drying with anhydrous sodium sulfate; organic phase was evaporated in vacuo. The crude product was purified using silica gel chromatography to obtain **4(a-o)**. Yield 75%–88%. White solid. **4a**: ^{1}H NMR (401 MHz, DMSO-d_6) δ 8.02 (m, 1H), 7.93 (dt, J = 6.4, 2.6 Hz, 1H), 7.76 (s, 1H), 7.45 (m, 2H), 3.68 (d, J = 4.7 Hz, 4H), 3.45 (m, 4H), 1.43 (s, 9H).

3.1.4 | General procedures for preparation of 5a-5o

To a solution of **4(a-o)** (1.0 mmol, 1.0 eq) in DCM (5 ml), m-CPBA (3.0 mmol, 3.0 eq) was added slowly in 30 min. After addition, the reaction was heated to 45℃ for 5 hr. Upon completion, solution was allowed to cool to room temperature. Saturated aqueous sodium bisulfite solution (50 ml) was added to the stirring solution for 15 min, subsequently adding saturated aqueous sodium bicarbonate solution (50 ml). The

mixture was quenched with water and extracted by DCM. Anhydrous sodium sulfate was used to remove water; organic phase was evaporated in vacuo. The crude product was purified using silica gel chromatography to obtain **5(a-o)**. White solid.

5a: Yield, 77%. ^{1}H NMR (401 MHz, DMSO-d6) δ 7.92 (d, *J* = 7.4 Hz, 1H), 7.81 (s, 1H), 7.75 (dd, *J* = 11.1, 3.7 Hz, 1H), 7.69 (t, *J* = 6.7 Hz, 2H), 3.58 (s, 4H), 3.40 (m, 4H), 1.42 (s, 9H).

5b: Yield, 81%. ^{1}H NMR (401 MHz, $CDCl_3$) δ 7.76 (d, *J* 8.1 Hz, 1H), 7.69 (d, *J* = 7.5 Hz, 1H), 7.24 (s, 1H), 3.58 (s, 4H), 3.97–3.38 (m, 4H), 1.42 (s, 9H).

5c: Yield, 79%. ^{1}H NMR (401 MHz, $CDCl_3$) δ 7.73 (dd, *J* 8.1 Hz, 1H), 7.60 (dd, *J* = 8.3 Hz, 2H), 7.52–7.41 (m, 4H), 3.58 (s, 4H), 3.97–3.38 (m, 4H), 1.42 (s, 9H).

5d: Yield, 77%. ^{1}H NMR (401 MHz, $CDCl_3$) δ 8.00 (1 H, s), 7.66 (1 H, s), 7.51 (1 H, dd, *J* = 8.5, 1.6 Hz), 7.44 (1 H, s), 3.78–3.70 (4 H, m), 3.57–3.49 (4 H, m), 1.48 (9 H, s).

5e: Yield, 80%. ^{1}H NMR (401 MHz, $CDCl_3$) δ 7.54 (1 H, dd, *J* = 8.4, 7.5 Hz), 7.21 (1 H, s), 7.07 (1 H, d, *J* = 8.5 Hz), 6.98 (1 H, d, *J* = 7.4 Hz), 3.67 (4 H, s), 3.54–3.50 (4 H, m), 1.47 (9 H, s).

5f: Yield, 64%. ^{1}H NMR (401 MHz, $CDCl_3$) δ 7.65 (1 H, d, *J* = 8.0 Hz), 7.45 (1 H, t, *J* = 7.7 Hz), 7.37 (1 H, d, *J* = 7.5 Hz), 7.22 (1 H, s), 3.70 (4 H, d, *J* = 22.9 Hz), 3.56–3.50 (4 H, m), 1.47 (11 H, s).

5g: Yield, 67%. ^{1}H NMR (401 MHz, $CDCl_3$) δ 7.68 (1 H, d, *J* = 8.1 Hz), 7.56 (1 H, dd, *J* = 8.1, 1.7 Hz), 7.42 (1 H, d, *J* = 1.6 Hz), 7.25 (1 H, s), 3.66 (4 H, s), 3.56–3.48 (4 H, m), 1.47 (9 H, s).

5h: Yield, 74%. ^{1}H NMR (401 MHz, $CDCl_3$) δ 7.72 (1 H, s), 7.58 (1 H, dd, *J* = 8.0, 1.8 Hz), 7.38 (1 H, d, *J* = 8.0 Hz), 7.29 (1 H, s), 3.67 (4 H, s), 3.56–3.49 (4 H, m), 1.47 (9 H, s).

5i: Yield, 65%. ^{1}H NMR (401 MHz, $CDCl_3$) δ 7.51 (2 H, dt, *J* = 8.1, 7.7 Hz), 7.32 (1 H, dd, *J* = 7.1, 0.9 Hz), 7.26 (1 H, s), 3.67 (4 H, s), 3.57–3.49 (4 H, m), 1.47 (9 H, s).

5j: Yield, 57%. ^{1}H NMR (401 MHz, $CDCl_3$) δ 7.54 (2 H, t, *J* = 7.9 Hz), 7.31 (1 H, d, *J* = 7.5 Hz), 7.10 (1 H, d, *J* = 8.4 Hz), 3.94 (3 H, s), 3.68 (4 H, s), 3.55–3.49 (4 H, m), 1.47 (9 H, s).

5k: Yield, 54%. ^{1}H NMR (401 MHz, $CDCl_3$) δ 7.36–7.29 (2 H, m), 7.27 (1 H, s), 7.06 (1 H, dd, *J* = 8.4, 2.3 Hz), 3.90 (3 H, s), 3.72–3.65 (4 H, m), 3.55–3.50 (4 H, m), 1.47 (9 H, s).

5l: Yield, 68%. ^{1}H NMR (401 MHz, $CDCl_3$) δ 7.54 (1 H, dd, *J* = 8.4, 7.5 Hz), 7.21 (1 H, s), 7.07 (1 H, d, *J* = 8.5 Hz), 6.98 (1 H, d, *J* = 7.4 Hz), 4.00 (3 H, s), 3.67 (4 H, s), 3.55–3.50 (4 H, m), 1.47 (9 H, s).

5m: Yield, 38%. ^{1}H NMR (401 MHz, $CDCl_3$) δ 7.74 (1 H, dd, *J* = 8.3, 4.6 Hz), 7.27 (2 H, q, *J* = 2.5 Hz), 7.24 (1 H, d, *J* = 2.8 Hz), 7.14 (1 H, dd, *J* = 7.7, 2.2 Hz), 3.66 (4 H, d, *J* = 11.6 Hz), 3.56–3.49 (4 H, m), 1.49 (9 H, s).

5n: Yield, 52%. ^{1}H NMR (401 MHz, $CDCl_3$) δ 7.74 (1 H, dd, *J* = 6.8, 1.1 Hz), 7.59 (2 H, td, *J* = 6.4, 1.2 Hz), 7.42 (1 H, dd, *J* = 6.4, 1.7 Hz), 7.26 (1 H, d, *J* = 0.6 Hz), 4.46–3.91 (2 H, m), 3.22 (2 H, d, *J* = 6.7 Hz), 2.51 (1 H, s), 1.76 (2 H, dd, *J* = 13.9, 3.8 Hz), 1.46 (9 H, s).

5o: Yield, 85%. ^{1}H NMR (401 MHz, $CDCl_3$) δ 7.87–7.78 (2 H, m), 7.46 (1 H, s), 7.42–7.36 (2 H, m), 4.51 (1 H, s), 4.40 (2 H, s), 3.75 (1 H, s), 3.13 (2 H, s), 2.04 (2 H, d, *J* = 10.6 Hz), 1.62 (1 H, s), 1.45 (9 H, s).

3.1.5 | General procedures for preparation of 6a-6o

To a solution of **5(a-o)** (1.0 mmol, 1.0 eq) in DCM (5 ml), TFA (0.5 ml) was added. Solution was stirred for 3 hr at room temperature. Upon completion, TFA and DCM were evaporated in vacuo. The residue was washed with ether; yellow oily solid was obtained without further purification.

3.1.6 | General procedures for preparation of 7a-7o

A mixture of 3,5,6-trimethylpyrazine-2-carboxylic acid (1.0 mmol, 1.0 eq), HATU (1.50 mmol 1.5 eq), DIEA (4.0 mmol, 4.0 eq) was stirred in anhydrous DMF (20 ml) for 15 min at room temperature; then, **6(a-o)** (1.0 mmol, 1.1 eq) was added. Reaction was stirred overnight at room temperature. Upon completion, DMF was removed by rotary evaporation under reduced pressure, the residue was dissolved in ethyl acetate (30 ml) and washed with saturated brine (10 ml × 3), collecting the organic layer and drying with anhydrous sodium sulfate, organic phase was evaporated in vacuo. The crude product was purified using silica gel chromatography. Pale yellow solid.

7a: Yield, 50%. ^{1}H NMR (401 MHz, $CDCl_3$) δ 7.74 (d, *J* = 5.6 Hz, 1H), 7.57 (s, 2H), 7.52 (m, 1H), 7.38 (s, 1H), 3.92 (d, *J* = 5.7 Hz, 2H), 3.84 (s, 2H), 3.74 (s, 2H), 3.41 (s, 2H), 2.59 (d, *J* = 8.6 Hz, 6H), 2.54 (s, 3H). ^{13}C NMR (101 MHz, $CDCl_3$) δ: 166.77, 158.67, 152.59, 148.70, 147.67, 144.11, 136.26, 134.41, 134.14, 131.72, 130.25, 129.26, 126.21, 121.81, 46.78, 42.64, 21.79, 21.10, 20.53. ESI-MS for $C_{21}H_{22}N_4O_4S$ *m/z*: 449.1197[*M* + Na]+.

7b: Yield, 49%. ^{1}H NMR (401 MHz, $CDCl_3$) δ 7.77 (d, *J* = 8.1 Hz, 1H), 7.69 (d, *J* = 7.4 Hz, 1H), 7.52 (s, 1H), 7.47 (t, *J* = 7.8 Hz, 1H), 3.94 (dd, *J* = 6.2, 3.6 Hz, 2H), 3.85 (s, 2H), 3.75 (s, 2H), 3.41 (s, 2H), 2.58 (d, *J* = 8.5 Hz, 6H), 2.53 (s, 3H). ^{13}C NMR (101 MHz, $CDCl_3$) δ: 166.84, 158.22, 152.55, 148.66, 147.80, 144.03, 140.52, 139.81, 134.20, 131.43, 131.23, 130.52, 126.37, 122.82, 46.53, 42.88, 21.79, 21.32, 20.32. ESI-MS for $C_{21}H_{21}ClN_4O_4S$ *m/z*: 483.0864 [*M* + Na]+.

7c: Yield, 37%. 1H NMR (401 MHz, CDCl3) δ 7.73 (d, *J* = 8.0 Hz, 1H), 7.61 (d, *J* = 7.3 Hz, 2H), 7.30 (s, 1H), 3.92 (d, *J* = 5.1 Hz, 2H), 3.83 (s, 2H), 3.73 (s, 2H), 3.40 (s, 2H), 2.53

(t, J = 8.6 Hz, 9H). ^{13}C NMR (101 MHz, $CDCl_3$) δ: 166.79, 158.37, 152.83, 148.73, 147.75, 143.93, 139.52, 138.26, 134.25, 132.03, 131.33, 130.50, 126.59, 122.43, 46.65, 43.10, 21.85, 21.36, 20.31. ESI-MS for $C_{21}H_{21}ClN_4O_4S$ *m/z*: 483.0865 [M + Na]+.

7d: Yield, 47%. ^{1}H NMR (401 MHz, DMSO-d6) 8.35 (1 H, s), 7.86 (1 H, d, J = 8.5 Hz), 7.78 (1 H, s), 7.60 (1 H, dd, J = 8.6, 1.5 Hz), 3.79 (4 H, s), 3.66 (2 H, s), 3.30 (2 H, d, J = 5.0 Hz), 2.48 (3 H, d, J = 4.5 Hz), 2.45 (3 H, d, J = 5.3 Hz), 2.40 (3 H, s). ^{13}C NMR (101 MHz, $CDCl_3$) δ: 166.87, 158.29, 152.56, 148.55, 147.68, 143.84, 138.44, 138.09, 137.53, 134.41, 132.10, 127.62, 126.99, 122.89, 46.83, 42.42, 21.89, 21.36, 20.39. ESI-MS for $C_{21}H_{21}ClN_4O_4S$ *m/z*: 483.0862 [M + Na]+.

7e: Yield, 56%. ^{1}H NMR (401 MHz, $CDCl_3$) 7.67 (1 H, d, J = 3.4 Hz), 7.49–7.42 (1 H, m), 7.37 (1 H, d, J = 7.5 Hz), 7.26 (1 H, s), 3.99–3.90 (2 H, m), 3.84 (2 H, s), 3.74 (2 H, s), 3.44–3.37 (2 H, m), 2.60–2.45 (9 H, m). ^{13}C NMR (101 MHz, $CDCl_3$) δ: 166.89, 158.31, 152.59, 148.69, 147.71, 143.97, 138.57, 138.13, 137.56, 134.23, 131.41, 127.73, 127.09, 122.42, 46.52, 42.12, 22.02, 21.33, 20.54. ESI-MS for $C_{21}H_{21}ClN_4O_4S$ *m/z*: 483.0865 [M + Na]+.

7f: Yield, 48%. ^{1}H NMR (401 MHz, $CDCl_3$) δ 7.70 (d, J = 8.2 Hz, 1H), 7.62 (d, J = 8.4 Hz, 1H), 7.55(m, 2H), 3.93 (s, 2H), 3.82 (s, 2H), 3.72 (s, 2H), 3.40 (s, 2H), 2.54 (t, J = 7.5 Hz, 9H). ^{13}C NMR (101 MHz, $CDCl_3$) δ: 166.94, 162.93, 158.68, 154.26, 150.31, 149.88, 136.21, 134.69, 133.85, 130.45, 128.61, 128.59, 128.43, 123.94, 46.57, 42.74, 21.69, 21.44, 20.43. ESI-MS for $C_{21}H_{21}BrN_4O_4S$ *m/z*: 527.0361 [M + Na]+.

7g: Yield, 64%. ^{1}H NMR (401 MHz, $CDCl_3$) δ 7.68 (2 H, d, J = 7.8 Hz), 7.57 (1 H, d, J = 9.1 Hz), 7.44 (1 H, s), 7.29 (1 H, s), 3.97–3.90 (2 H, m), 3.83 (2 H, s), 3.72 (5 H, dd, J = 14.0, 7.0 Hz), 2.60–2.46 (9 H, t). ^{13}C NMR (101 MHz, $CDCl_3$) δ: 166.95, 160.90, 160.68, 157.26, 152.71, 149.04, 134.95, 134.24, 133.99, 130.11, 129.35, 128.88, 128.66, 123.07, 46.53, 43.80, 21.79, 21.56, 20.30. ESI-MS for $C_{21}H_{21}BrN_4O_4S$ *m/z*: 527.0354 [M + Na]+.

7h: Yield, 65%. ^{1}H NMR (401 MHz, $CDCl_3$) δ 7.72 (1 H, s), 7.59 (1 H, dd, J = 8.0, 1.7 Hz), 7.39 (1 H, d, J = 8.0 Hz), 7.33 (1 H, s), 3.96–3.88 (2 H, m), 3.81 (2 H, d, J 14.6), 3.73 (2 H, t, J = 6.9 Hz), 3.45–3.36 (2 H, m), 2.55 (9 H, t, J = 7.7 Hz). ^{13}C NMR (101 MHz, $CDCl_3$) δ: 166.89, 163.71, 152.55, 148.67, 147.80, 144.14, 141.67, 137.25, 136.38, 128.62, 125.80, 125.21, 124.94, 120.18, 46.67, 41.86, 21.99, 21.41, 20.57. ESI-MS for $C_{21}H_{21}BrN_4O_4S$ *m/z*: 527.0364 [M + Na]+.

7i: Yield, 42%. ^{1}H NMR (401 MHz, $CDCl_3$) δ 7.64 (t, J = 9.2 Hz, 2H), 7.40 (d, J = 8.3 Hz 1H), 7.35 (s, 1H), 3.95 (s, 2H), 3.84 (s, 2H), 3.76 (s, 2H), 3.40 (s, 2H), 2.55 (t, J = 8.0 Hz, 9H). ^{13}C NMR (101 MHz, $CDCl_3$) δ: 166.82, 158.16, 152.57, 148.70, 147.71, 144.03, 139.73, 132.48, 131.80, 130.33, 123.85, 118.40, 118.08, 113.82, 46.52, 42.10, 21.81, 21.09, 20.78. ESI-MS for $C_{21}H_{21}BrN_4O_4S$ *m/z*: 527.0355 [M + Na]+.

7j: Yield, 53%. ^{1}H NMR (401 MHz, $CDCl_3$) δ(ppm): 7.53 (2 H, t, J = 7.9 Hz), 7.31 (1 H, d, J = 7.5 Hz), 7.09 (1 H, d, J = 8.4 Hz), 3.67 (4 H, s), 3.54–3.48 (4 H, m), 2.55 (9 H, t, J = 7.9 Hz). ^{13}C NMR (101 MHz, $CDCl_3$) δ: 166.81, 164.16, 158.63, 152.47, 148.58, 147.57, 144.20, 139.23, 131.67, 131.50, 127.49, 123.26, 115.39, 112.51, 55.98, 46.92, 46.37, 42.80, 41.91, 21.92, 21.38, 20.47. ESI-MS for $C_{22}H_{24}N_4O_5S$ *m/z*: 479.1358 [M + Na]+.

7k: Yield, 44%. ^{1}H NMR (401 MHz, $CDCl_3$) δ 7.66 (1 H, d, J = 8.5 Hz), 7.26–7.24 (1 H, m), 7.01 (1 H, dd, J = 8.4, 1.8 Hz), 6.92 (1 H, s), 3.93 (2 H, dd, J = 6.3, 3.5 Hz), 3.90 (3 H, s), 3.84 (2 H, s), 3.73 (2 H, t, J = 6.9 Hz), 3.42–3.36 (2 H, m), 2.52 (9 H, t, J = 7.6 Hz). ^{13}C NMR (101 MHz, $CDCl_3$) δ: 166.73, 163.08, 158.42, 152.49, 148.69, 147.57, 144.14, 138.19, 135.99, 133.12, 127.45, 121.14, 119.24, 107.90, 56.23, 46.81, 41.94, 21.91, 21.30, 20.36. ESI-MS for $C_{22}H_{24}N_4O_5S$ *m/z*: 479.1355 [M + Na]+.

7l: Yield, 68%. ^{1}H NMR (401 MHz, $CDCl_3$) δ 7.57–7.51 (1 H, m), 7.24 (1 H, s), 7.07 (1 H, d, J = 8.5 Hz), 6.98 (1 H, d, J = 7.3 Hz), 4.00 (3 H, s), 3.93 (2 H, dd, J = 6.4, 3.6 Hz), 3.83 (2 H, s), 3.73 (2 H, t, J = 7.0 Hz), 3.41–3.37 (2 H, m), 2.52 (9 H, t, J = 7.9 Hz). ^{13}C NMR (101 MHz, $CDCl_3$) δ: 166.69, 158.71, 155.58, 152.51, 148.68, 147.54, 144.12, 138.61, 136.16, 131.41, 131.07, 121.23, 118.27, 115.14, 56.43, 46.69, 42.05, 21.77, 21.27, 20.29. ESI-MS for $C_{22}H_{24}N_4O_5S$ *m/z*: 479.1357 [M + Na]+.

7m: Yield, 38%. ^{1}H NMR (401 MHz, $CDCl_3$) δ 7.75 (1 H, dd, J = 8.0, 4.7 Hz), 7.29 (2 H, q, J = 2.5 Hz), 7.15 (1 H, d, J = 7.7 Hz), 3.93 (2 H, dd, J = 6.4, 3.6 Hz), 3.83 (2 H, s), 3.76–3.71 (2 H, m), 3.42–3.37 (2 H, m), 2.53 (9 H, t, J = 7.8 Hz). ^{13}C NMR (101 MHz, $CDCl_3$) δ: 166.96, 160.12, 155.73, 148.56, 147.65, 143.51, 139.46, 139.26, 135.36, 133.06, 130.98, 130.40, 125.98, 122.43, 46.29, 42.93, 21.85, 21.39, 20.58. ESI-MS for $C_{21}H_{21}FN_4O_4S$ *m/z*: 467.1260 [M + Na]+.

7n: Yield, 55%. ^{1}H NMR (401 MHz, $CDCl_3$) δ 8.02 (1 H, d, J = 8.3 Hz), 7.75 (1 H, dd, J = 6.9, 1.0 Hz), 7.60 (2 H, td, J = 6.4, 1.2 Hz), 7.43 (1 H, dd, J = 6.4, 1.7 Hz), 4.62 (1 H, s), 4.22 (2 H, dd, J = 7.7, 3.6 Hz), 2.90 (3 H, s), 2.55 (6H, d, J = 10.4 Hz), 2.14 (2 H, d, J = 10.5), 1.82 (2 H, s), 1.68 (2 H, d, J = 9.5 Hz). ^{13}C NMR (101 MHz, $CDCl_3$) δ: 164.38, 158.14, 154.39, 151.37, 147.71, 138.84, 138.49, 136.33, 133.94, 131.42, 131.06, 129.56, 125.92, 121.61, 46.55, 46.26, 41.74, 32.88, 31.67, 22.87, 22.02, 21.35. ESI-MS for $C_{22}H_{24}N_4O_4S$ *m/z*: 463.1423 [M + Na]+.

7o: Yield, 52%. ^{1}H NMR (401 MHz, $CDCl_3$) δ 7.73 (1 H, dd, J = 6.8, 1.1 Hz), 7.56 (2 H, td, J = 6.4, 1.2 Hz), 7.41 (1 H, dd, J = 6.4, 1.7 Hz), 7.25 (1 H, d, J = 0.6 Hz), 4.45–3.93 (2 H, m), 3.21 (2 H, d, J = 6.7 Hz), 2.51 (1 H, s), 1.77 (2 H, dd, J = 13.9, 3.8 Hz), 2.55 (9 H, t, J = 7.8 Hz). ^{13}C NMR (101 MHz, $CDCl_3$) δ: 166.47, 157.24, 155.39, 150.27, 144.55,

141.24, 139.29, 139.12, 131.24, 130.22, 131.89, 127.64, 125.32, 122.21, 49.69, 45.24, 40.38, 32.11, 23.01, 22.17, 21.89. ESI-MS for $C_{21}H_{22}N_4O_4S$ *m/z*: 449.1261 [*M* + Na]+.

3.1.7 | General procedures for preparation of 8a-8m

A mixture of **6(a-o)** (1.0 mmol, 1.0 eq), KI (0.01 mmol, 0.01 eq), TEA (3.0 mmol, 3.0 eq) were stirred in CH_3CN (20 ml) for 15 min at room temperature; then, 2-(bromomethyl)-3,5, 6-trimethylpyrazine (1.1 mmol, 1.1 eq) was added. Reaction was heated to 80°C. 1 hr later, CH_3CN was removed by rotary evaporation under reduced pressure, the residue was dissolved in DCM (30 ml) and washed with saturated brine (10 ml × 3), collecting the organic layer and drying with anhydrous sodium sulfate, and organic phase was evaporated in vacuo. The crude product was purified using silica gel chromatography. White solid.

8a: Yield, 46%. ^{1}H NMR (401 MHz, $CDCl_3$) δ 7.73 (d, *J* = 6.8 Hz, 1H), 7.58 (m, 2H), 7.42 (m, 1H), 7.28 (s, 1H), 3.70 (d, *J* = 6.2 Hz, 6H), 2.60 (s, 4H), 2.55 (s, 3H), 2.49 (d, *J* = 2.2 Hz, 6H). ^{13}C NMR (101 MHz, $CDCl_3$) δ: 158.17, 149.93, 149.73, 148.29, 146.98, 138.59, 136.32, 134.08, 131.42, 131.19, 129.40, 125.94, 121.65, 59.91, 47.44, 42.45, 21.53, 21.43, 20.88. ESI-MS for $C_{21}H_{24}N_4O_3S$ *m/z*: 435.1461 [*M* + Na]+.

8b: Yield, 48%. ^{1}H NMR (401 MHz, $CDCl_3$) δ 7.75 (d, *J* = 8.1 Hz, 1H), 7.68 (d, *J* = 7.5 Hz, 1H), 7.45 (dd, *J* = 9.1, 6.5 Hz, 2H), 3.72 (s, 6H), 2.65 (m, 4H), 2.59 (s, 3H), 2.50 (s, 6H). ^{13}C NMR (101 MHz, $CDCl_3$) δ: 158.26, 149.73, 149.71, 148.38, 146.65, 138.87, 136.55, 134.21, 131.12, 131.05, 129.65, 126.21, 121.76, 60.59, 47.49, 43.20, 21.96, 21.53, 20.23. ESI-MS for $C_{21}H_{23}ClN_4O_3S$ *m/z*: 469.2372 [*M* + Na]+.

8c: Yield, 39%. ^{1}H NMR (401 MHz, $CDCl_3$) δ 7.70 (d, *J* = 8.1 Hz, 1H), 7.62 (d, *J* = 7.5 Hz, 2H), 7.28 (s, 1H), 3.74 (s, 6H), 2.69 (m, 4H), 2.56 (s, 3H), 2.49 (d, *J* = 2.1 Hz, 6H). ^{13}C NMR (101 MHz, $CDCl_3$) δ: 158.19, 150.03, 149.93, 148.81, 147.64, 139.24, 136.66, 134.28, 132.0, 131.79, 128.41, 125.84, 122.31, 60.96, 47.39, 42.41, 21.87, 21.65, 20.87. ESI-MS for $C_{21}H_{24}N_4O_3S$ *m/z*: 469.2372 [*M* + Na]+.

8d: Yield, 47%. ^{1}H NMR (401 MHz, $CDCl_3$) 8.35 (1 H, s), 7.87 (1 H, d, *J* = 8.4 Hz), 7.77 (1 H, s), 7.60 (1 H, dd, *J* = 8.8, 1.9 Hz), 3.79 (4 H, s), 3.78 (2 H, s), 3.65 (2 H, s), 3.30 (2 H, d, *J* = 5.5 Hz), 2.50 (3 H, d, *J* = 4.5 Hz), 2.46 (3 H, d, 5.3), 2.41 (3 H, s). ^{13}C NMR (101 MHz, $CDCl_3$) δ: 158.67, 150.26, 149.65, 148.31, 146.33, 138.67, 136.68, 134.54, 131.29, 131.11, 128.20, 125.91, 121.11, 61.13, 48.01, 43.55, 21.56, 21.54, 20.56. ESI-MS for $C_{21}H_{24}N_4O_3S$ *m/z*: 469.2372 [*M* + Na]+.

8e: Yield, 56%. ^{1}H NMR (401 MHz, $CDCl_3$) 7.65 (1 H, d, *J* = 3.8), 7.47–7.40 (1 H, m), 7.35 (1 H, d, *J* = 7.7 Hz), 7.25 (1 H, s), 3.99–3.91 (2 H, m), 3.84 (2 H, s), 3.74 (2 H, s), 3.44–3.37 (2 H, m), 2.60–2.45 (9 H, m). ^{13}C NMR (101 MHz, $CDCl_3$) δ: 158.36, 149.64, 149.37, 148.96, 146.67, 138.32, 136.14, 134.43, 131.54, 131.36, 129.40, 125.64, 121.34, 60.31, 47.64, 42.21, 21.43, 21.41, 20.45. ESI-MS for $C_{21}H_{24}N_4O_3S$ *m/z*: 469.2372 [*M* + Na]+.

8f: Yield, 48%. ^{1}H NMR (401 MHz, $CDCl_3$) δ 7.64 (d, *J* = 7.3 Hz, 1H), 7.58 (d, *J* = 7.8 Hz, 1H), 7.53 (d, *J* = 7.7 Hz, 1H), 7.50 (s, 1H), 3.70 (s, 6H), 2.63 (s, 4H), 2.57 (s, 3H), 2.49 (d, *J* = 1.9 Hz, 6H). ^{13}C NMR (101 MHz, $CDCl_3$) δ: 157.26, 150.13, 149.99, 149.74, 147.80, 146.57, 140.11, 139.82, 138.11, 136.85, 132.52, 129.36, 119.96, 61.26, 53.04, 46.53, 22.72, 21.54, 20.78. ESI-MS for $C_{21}H_{23}BrN_4O_3S$ *m/z*: 513.1667 [*M* + Na]+.

8g: Yield, 64%. ^{1}H NMR (401 MHz, $CDCl_3$) δ 7.68 (2 H, d, *J* = 7.9 Hz), 7.56 (1 H, d, *J* = 9.0 Hz), 7.44 (1 H, s), 7.29 (1 H, s), 3.95–3.91 (2 H, m), 3.83–3.76 (4 H, m), 3.72 (4 H, dd, *J* = 14.9, 7.1 Hz), 2.61–2.45 (9 H, t). ^{13}C NMR (101 MHz, $CDCl_3$) δ: 157.54, 149.89, 149.81, 149.74, 147.68, 146.14, 140.36, 139.72, 138.36, 136.65, 132.31, 129.28, 120.14, 61.12, 52.95, 46.78, 22.81, 21.24, 20.96. ESI-MS for $C_{21}H_{23}BrN_4O_3S$ *m/z*: 513.1666 [*M* + Na]+.

8h: Yield, 65%. ^{1}H NMR (401 MHz, $CDCl_3$) δ 7.72 (1 H, s), 7.59 (1 H, dd, *J* = 8.0, 1.7 Hz), 7.38 (1 H, d, *J* = 8.0 Hz), 7.33 (1 H, s), 3.93–3.85 (2 H, m), 3.80 (2 H, d, *J* = 14.6 Hz), 3.73 (2 H, t, *J* = 6.9 Hz), 3.72 (2 H, s),3.45–3.37 (2 H, m), 2.54 (9 H, t, *J* = 7.7 Hz). ^{13}C NMR (101 MHz, $CDCl_3$) δ: 157.78, 149.97, 149.87, 149.64, 147.24, 146.31, 140.25, 139.73, 138.31, 136.63, 132.44, 129.66, 119.89, 62.20, 52.68, 45.29, 23.12, 22.03, 21.05. ESI-MS for $C_{21}H_{23}BrN_4O_3S$ *m/z*: 513.1667 [*M* + Na]+.

8i: Yield, 47%. ^{1}H NMR (401 MHz, $CDCl_3$) δ 7.50 (dt, *J* = 15.7, 7.9 Hz, 2H), 7.31 (d, *J* = 7.1 Hz, 3H), 7.23 (s, 1H), 7.23 (s, 1H), 3.76 (s, 6H), 2.71 (s, 4H), 2.58 (s, 3H), 2.49 (d, *J* = 1.6 Hz, 6H). ^{13}C NMR (101 MHz, $CDCl_3$) δ: 158.21, 149.37, 149.31, 148.64, 147.54, 146.15, 140.31, 139.76, 138.35, 136.64, 132.27, 129.38, 120.16, 61.14, 52.69, 46.78, 22.34, 21.34, 20.99. ESI-MS for $C_{21}H_{23}BrN_4O_3S$ *m/z*: 513.1667 [*M* + Na]+.

8j: Yield, 53%. ^{1}H NMR (401 MHz, $CDCl_3$) δ 7.51 (2 H, t, *J* = 7.9 Hz), 7.31 (1 H, d, *J* = 7.5 Hz), 7.11 (1 H, d, *J* = 8.4 Hz), 3.94 (3 H, s), 3.73 (6 H, s), 3.47 (2 H, s), 2.66 (2 H, s), 2.54 (9 H, t, *J* = 7.9 Hz). ^{13}C NMR (101 MHz, $CDCl_3$) δ: 166.48, 158.95, 154.86, 152.37, 148.51, 147.10, 144.16, 137.41, 135.70, 133.72, 128.88, 117.49, 116.32, 113.14, 60.60, 56.21, 46.99, 41.87, 21.93, 21.41, 20.48. ESI-MS for $C_{22}H_{26}N_4O_4S$ *m/z*: 481.1302 [M + K]+.

8k: Yield, 44%. ^{1}H NMR (401 MHz, $CDCl_3$) δ 7.35 (2 H, t, *J* = 4.1 Hz), 7.27 (1 H, d, *J* = 1.8 Hz), 7.07 (1 H, dd, *J* = 8.4, 2.3 Hz), 3.92 (2 H, dd, *J* = 6.4, 3.4 Hz), 3.88–3.82 (4 H, m), 3.74 (2 H, dd, *J* = 8.7, 3.7 Hz), 3.41–3.36 (2 H, m), 2.54(9 H, t, *J* = 7.9 Hz). ^{13}C NMR (101 MHz, $CDCl_3$) δ: 162.71, 158.53, 150.42, 149.84, 149.58, 148.23, 146.87,

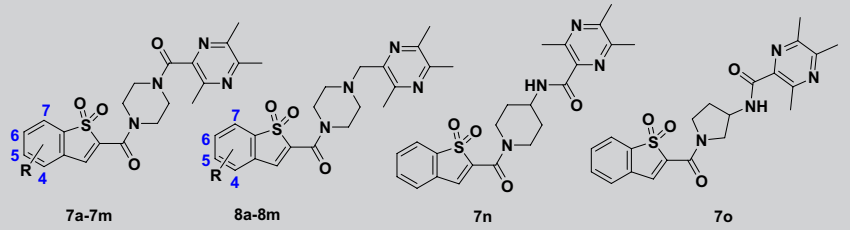

TABLE 1 Antiproliferation activity of compounds **7a-7o** and **8a-8m**

		Antiproliferative activity ($IC_{50} \pm SD$, μM)			
Compounds	**R**	**HCT116**	**MCF-7**	**MDA-MB-231**	**HepG2**
7a	H	>10	>10	>10	>10
7b	4-Cl	5.08 ± 0.15	4.31 ± 0.26	4.69 ± 0.13	4.90 ± 0.17
7c	5-Cl	>10	>10	>10	>10
7d	6-Cl	>10	3.24 ± 0.17	>10	>10
7e	7-Cl	>10	9.54 ± 0.98	>10	>10
7f	4-Br	6.44 ± 0.61	3.29 ± 0.08	4.86 ± 0.27	>10
7g	5-Br	5.81 ± 0.04	3.35 ± 0.11	6.41 ± 0.21	>10
7h	6-Br	>10	>10	>10	>10
7i	7-Br	>10	>10	>10	>10
7j	4-OCH_3	>10	3.58 ± 0.20	3.58 ± 0.03	5.81 ± 0.09
7k	6-OCH_3	>10	>10	>10	>10
7l	7-OCH_3	>10	>10	>10	4.81 ± 0.05
7m	5-F	6.65 ± 0.12	3.85 ± 0.05	>10	6.12 ± 0.20
7n	H	>10	>10	>10	>10
7o	H	>10	>10	>10	>10
8a	H	4.93 ± 0.04	3.45 ± 0.09	4.82 ± 0.13	>10
8b	4-Cl	2.67 ± 0.05	1.50 ± 0.02	2.20 ± 0.16	5.94 ± 0.38
8c	5-Cl	7.72 ± 0.91	3.20 ± 0.25	7.86 ± 0.59	>10
8d	6-Cl	>10	3.57 ± 0.06	8.02 ± 0.24	>10
8e	7-Cl	3.78 ± 0.03	2.21 ± 0.07	2.86 ± 0.36	>10
8f	4-Br	3.91 ± 0.39	4.26 ± 0.09	4.44 ± 0.41	>10
8g	5-Br	3.06 ± 0.51	3.52 ± 0.06	5.39 ± 0.16	4.26 ± 0.36
8h	6-Br	>10	>10	>10	>10
8i	7-Br	3.36 ± 0.33	2.42 ± 0.02	3.42 ± 0.07	4.67 ± 0.28
8j	4-OCH_3	4.93 ± 0.05	4.56 ± 0.41	7.41 ± 0.88	4.80 ± 0.67
8k	6-OCH_3	>10	>10	>10	>10
8l	7-OCH_3	3.05 ± 0.26	5.12 ± 0.31	5.40 ± 0.07	4.26 ± 0.05
8m	5-F	6.69 ± 0.62	5.22 ± 0.21	5.96 ± 0.23	>10
Stattic	\	1.71 ± 0.06	2.08 ± 0.07	3.90 ± 0.04	6.75 ± 0.15

Note: IC_{50} values represent the mean ± *SD* for each compound based on three independent experiments.

138.27, 132.13, 126.86, 121.49, 119.15, 107.32, 61.26, 56.21, 46.53, 43.10, 21.50, 21.42, 20.85. ESI-MS for $C_{22}H_{26}N_4O_4S$ *m/z*: 465.1567 [*M* + Na]+.

8l: Yield, 68%. ^{1}H NMR (401 MHz, $CDCl_3$) δ 7.52 (1 H, dd, *J* = 8.4, 7.5 Hz), 7.18 (1 H, s), 7.05 (1 H, d, *J* = 8.5 Hz), 6.98 (1 H, d, *J* = 7.3 Hz), 3.93 (2 H, dd, *J* = 6.4, 3.6 Hz),3.90 (3 H, s), 3.83 (2 H, s),3.76 (2 H,s), 3.73 (2 H, t, *J* = 7.0 Hz), 3.41–3.37 (2 H, m), 2.52 (9 H, t, *J* = 7.9 Hz). ^{13}C NMR (101 MHz, $CDCl_3$) δ: 162.87, 158.63, 150.29, 149.91, 149.90, 148.33, 146.67, 138.81, 132.22, 126.62, 121.45, 119.54, 107.37, 61.25, 57.31, 46.29, 42.59, 21.90, 21.68, 20.75. ESI-MS for $C_{22}H_{26}N_4O_4S$ *m/z*: 465.1565 [*M* + Na]+.

8m: Yield, 38%. ^{1}H NMR (401 MHz, $CDCl_3$) δ 7.76 (1 H, dd, J = 8.1, 46 Hz), 7.29 (2 H, q, J = 2.3 Hz), 7.15 (1 H, d, J = 7.5 Hz), 3.94 (2 H, dd, J = 6.4, 3.5 Hz), 3.83 (2 H, s), 3.76–3.71 (2 H, m), 3.40–3.36 (4 H, m), 2.54 (9 H, t, J = 7.8 Hz). ^{13}C NMR (101 MHz, $CDCl_3$) δ: 160.12, 153.21, 149.70, 148.23, 144.44, 139.21, 139.55, 135.66, 133.71, 130.68, 125.98, 122.24, 61.54, 46.21, 42.64, 21.55, 21.10, 20.18. ESI-MS for $C_{21}H_{21}FN_4O_4S$ m/z: 453.1278 [M + Na]+.

3.2 | In vitro cell growth inhibition activities

The antiproliferation activity of all synthetic compounds was evaluated using four cell lines (HCT-116, MCF-7, MDA-MB-231, and HepG2). Stattic was used as positive control. As shown in Table 1, the anticancer activity of each compound was presented as IC_{50}. No inhibition was observed in **7n** and **7o** groups, indicating that piperazine linker is more appropriate for promoting activity. **8a-8m** showed significantly better antiproliferation activity than **7a-7o**, reveling the flexibility of the methylene group between ligustrazine and piperazine. The substituents in the benzene ring have a significant effect on the activity, with the substituents for C6 and C7 positions in benzene leading directly to the loss of activity. However, the species of benzene substituents have little impacts on activity. Among these compounds, **8b** exhibited excellent activities against HepG2, MCF-7, MDA-MB-231, and HCT116 cancer cell lines with IC_{50} ranging from 1.50 to 5.94 μM. Considering the potent anticancer activity, we performed further mechanistic studies based on **8b**.

3.3 | Compound 8b induced apoptosis in cancer cells

To explore the ability of compound **8b** to induce apoptosis, Annexin V-FITC/PI staining assay was performed. The result of flow cytometry assay showed that compound **8b** can induce apoptosis in a dose-dependent manner in cancer cells (Figure 2a). At the concentration of 2.5 μM, the apoptosis rates of MDA-MB-231 cells, HepG2 cells, MCF-7 cells, and HCT116 cells reached to 30.90%, 37.33%, 6.43%, and 21.90%, respectively (Figure 1b).

3.4 | Compound 8b induced G2-phase arrest in cancer cells

We investigated the cell cycle effects of compound **8b** on HepG2, MCF-7 and HCT116 cells by flow cytometry. As shown in Figure 3, the percentage of cells in G2 phase increased significantly after treatment. These data revealed that compound **8b** could cause G2 arrest in HepG2, MCF-7 and HCT116 cells in a dose-dependent manner.

3.5 | Compound 8b induced the generation of ROS in cancer cells

The induction of apoptosis through elevated ROS levels has been highlighted as the core of targeted cancer therapy. Considering the ROS generation function of ligustrazine (Yu et al., 2018), we detected the ROS level in HepG2 cells and MCF-7 cells. As shown in Figure 4, the ROS level was

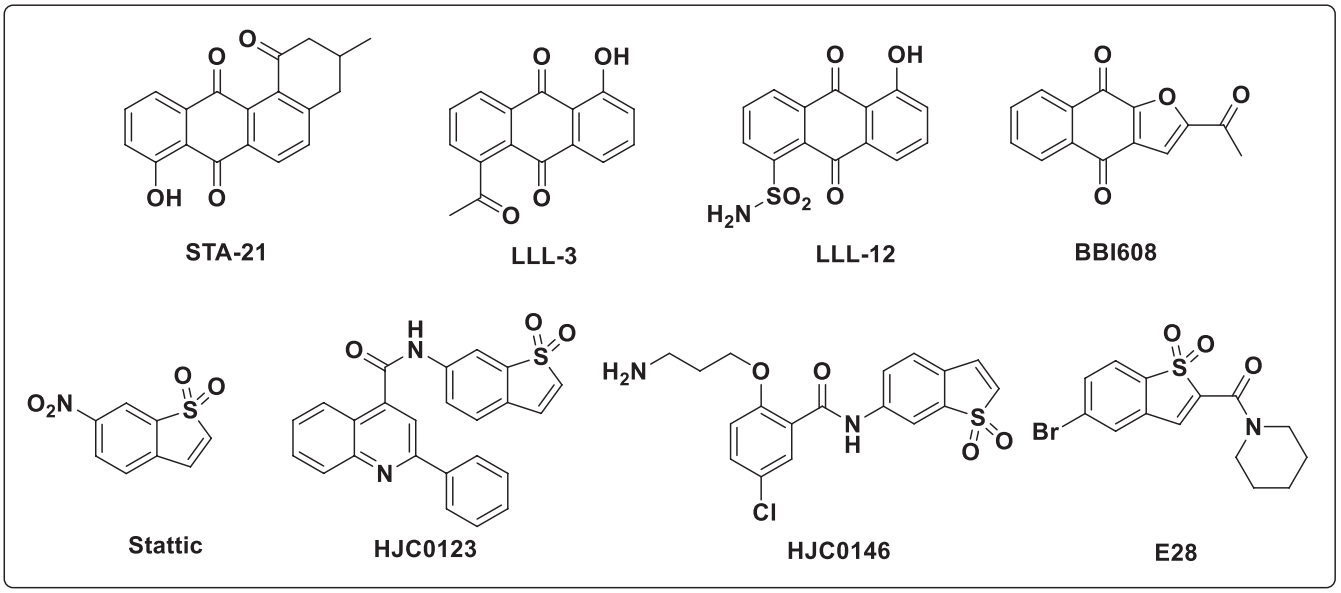

FIGURE 1 Chemical structures of SH2 domain targeting STAT3 inhibitors

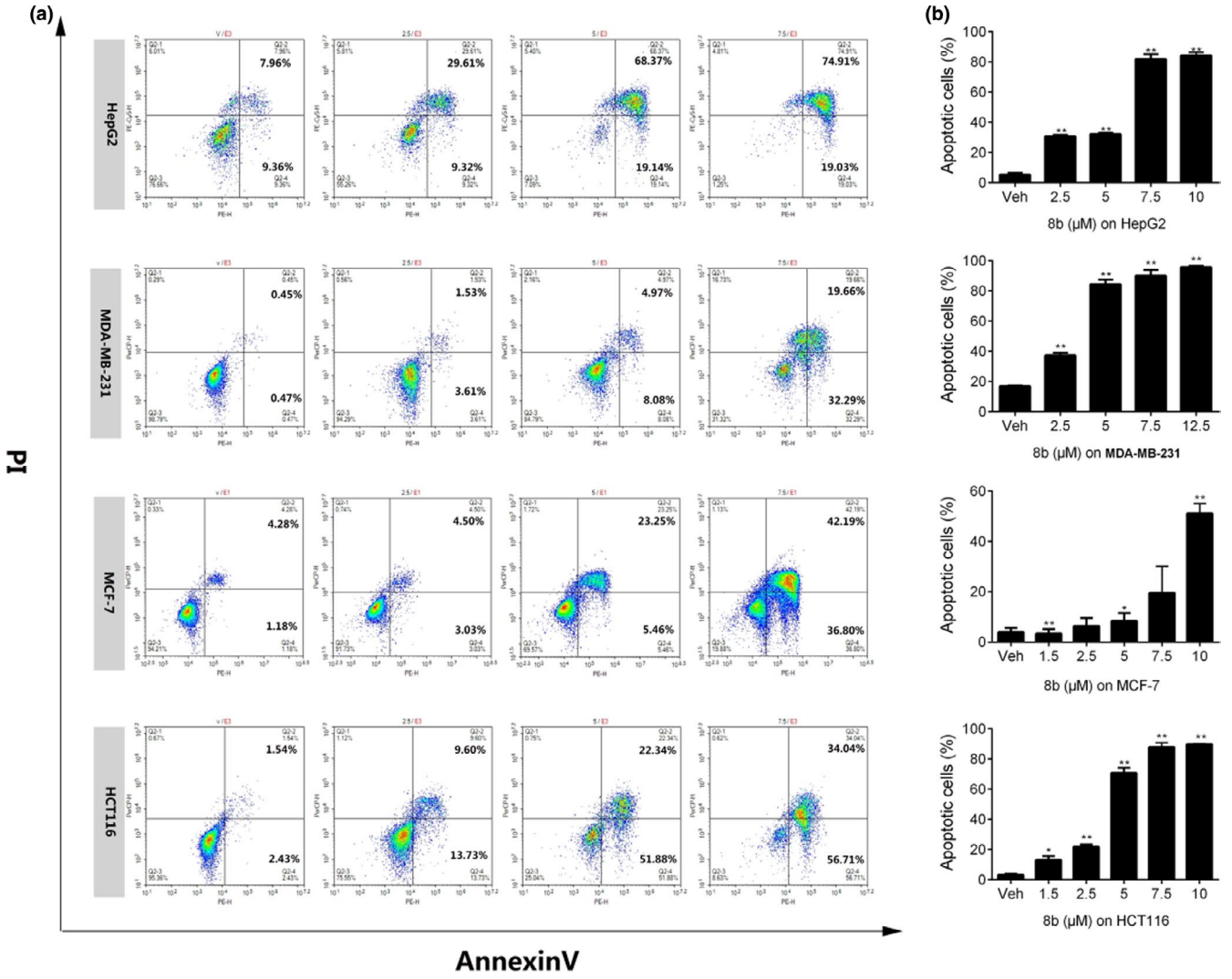

FIGURE 2 Compound **8b** induced apoptosis in cancer cells. (a) HepG2 cell line, MDA-MB-231 cell line, MCF-7 cell line, and HCT116 cell line were treated with compound **8b** at tested concentration for 24 hr and analyzed by flow cytometer. (b) The ratio of apoptosis cells in HepG2, MDA-MB-231, MCF-7, and HCT116, respectively. (*$p < .05$, **$p < .01$, compared with the vehicle group)

significantly up-regulated in MCF-7 cells and HepG2 cells when compared to vehicle, indicating that the introduction of ligustrazine empowered **8b** to generate active oxygen, thereby resulting in significant cancer cells apoptosis.

3.6 | Compound 8b caused the loss of mitochondrial membrane potential (Δψ m)

It has been found that many cancer-derived cells (lung cancer, breast cancer, melanomas) possess a higher mitochondrial membrane potential than normal cells (Bonnet et al., 2007; Chen, 1988; Hockenbery, 2002; Kroemer & Pouyssegur, 2008). In contrast, loss of mitochondrial membrane potential is a sign of the early apoptosis mediated by the mitochondrial pathway (Ye et al., 2017). To investigate the mechanism of compound **8b**-induced apoptosis, we measured the Δψm in HepG2 cells and MCF-7 cells. As shown in Figure 5, compound **8b** induced the loss of mitochondrial membrane potential in a dose-dependent manner, indicating the apoptosis of above cancer cells may be caused by the change of mitochondrial membrane potential.

3.7 | Compound 8b inhibits the activation of STAT3 and regulates the expression of proteins related to apoptosis, cell cycle, and DNA damage in HepG2

Western blot assay was conducted to exam whether compound **8b** functioned as an STAT3 inhibitor. As shown in Figure 6a, the phosphorylation of STAT3(Tyr705) was significantly blocked at 2.5 μM. Meanwhile, E-cadherin and

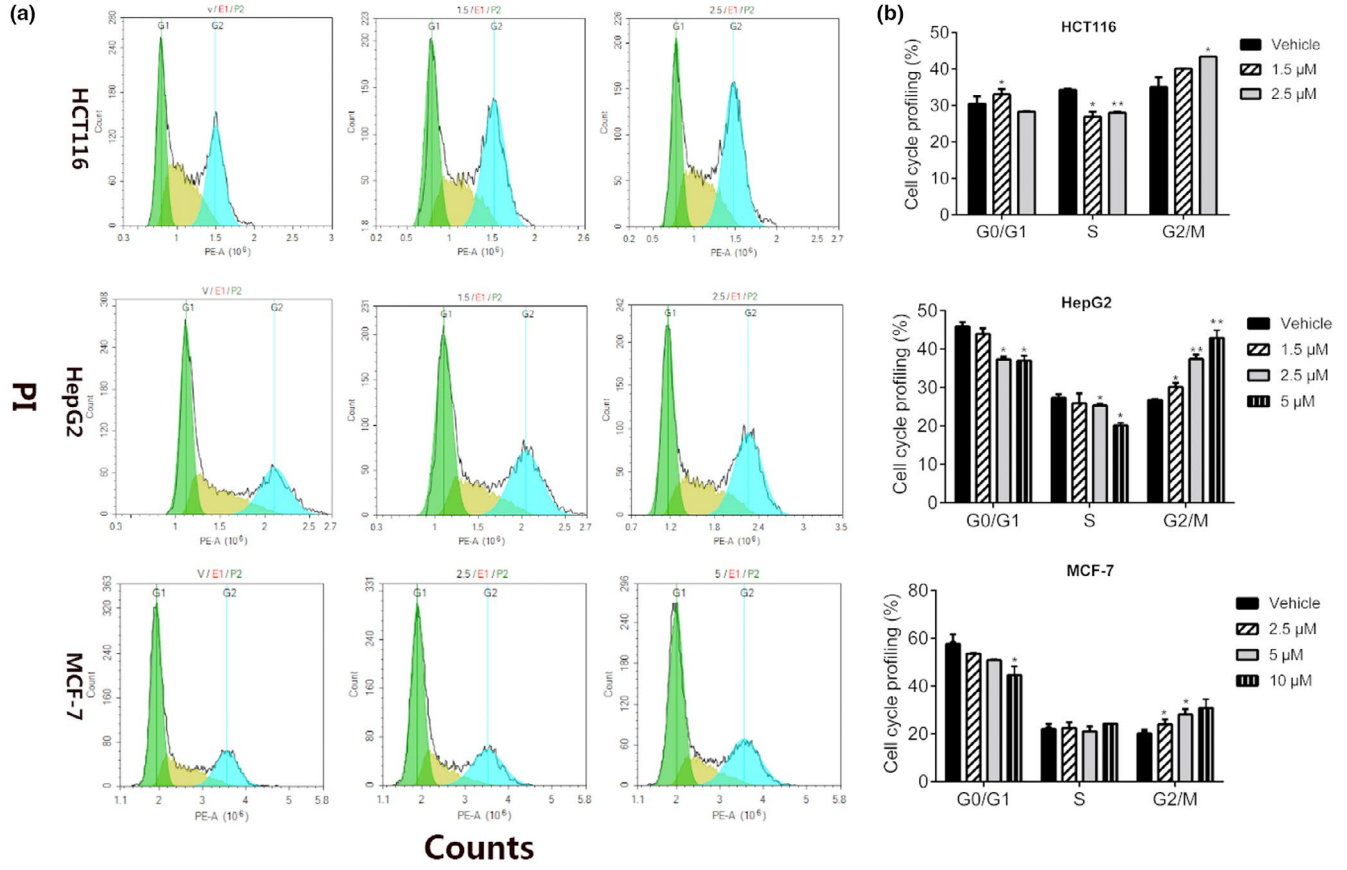

FIGURE 3 Compound **8b** induced G2-phase arrest in cancer cells. (a) HCT116 cell line, HepG2 cell line, and MCF-7 cell line were treated with compound **8b** at tested concentration for 24 hr and analyzed by flow cytometer. (b) The ratio of cell cycle phase in HCT116, HepG2, and MCF-7 respectively. (*$p < .05$, **$p < .01$, compared with the vehicle group)

vimentin proteins associated with migration and invasion represented uptrend and downtrend, respectively, validating the antiproliferation abilities of **8b** in cancer cells. p53 protein is the product of a critical tumor-suppressor gene; the activation of p53 can result in DNA damage, apoptosis, and cell cycle arrest in cancer cells. This demonstrated that 8b could effectively upregulate the expression level of p53 in HepG2 cells. To further investigate the anti-tumor mechanism, we determined the expression of proteins related to cell cycle, DNA damage, and apoptosis. As shown in Figure 6b, **8b** reduced the expression of p-CDC2 and increased the expression of cylin B, which were consistent with G2/M arrest results in 3.4. Besides, **8b** promoted the expression of γ2HAX, demonstrating **8b** increased the DNA double-strand breaks. Cleaved caspase 3, Bcl-2, and Bax are pivotal proteins of intrinsic apoptosis. In Figure 6c, the ratio of Bax/Bcl-2 and the expression of cleaved caspase 3 were significantly increased dose dependently, indicating the apoptotic pathway might a vital role in **8b**-induced cancer cell death. Western blot assays have proved that compound **8b** regulates the expression level of p-STAT3; thus, we carried out dual-luciferase reporter assays to verify whether compound **8b** was worked in a targeted manner. The ratio of Firefly luciferase activity and Renilla luciferase activity can reflect that constitutive STAT3 transcription activity was blocked by **8b**-treated HepG2 cells; compound **8b** had stronger inhibitory ability then Stattic (Figure 6c). In general, all these results proved that compound **8b** is an effective inhibitor targeting STAT3.

3.8 | Molecular docking study

To figure out the binding model of **8b** to STAT3, we docked compound **8b** to the SH2 domain (PDB:1BG1). As shown in Figure 7, the BTP part of compound **8b** binds to pY-X tightly. On this basis, the piperazine ring elongates the molecular length; methylene turns and provides ligustrazine fragment excellent flexibility and angle to bind into pY cavity. Generally, compound **8b** forms hydrogen bonds with Lys591 and Ser636, and Pi-Pi conjugations with other amino acid residues can also be found.

4 | CONCLUSION

In this study, we successfully designed and synthesized a series of novel inhibitors based on benzo[b]thiophene 1,1-dioxide scaffold. Compound **8b** was found to be the most

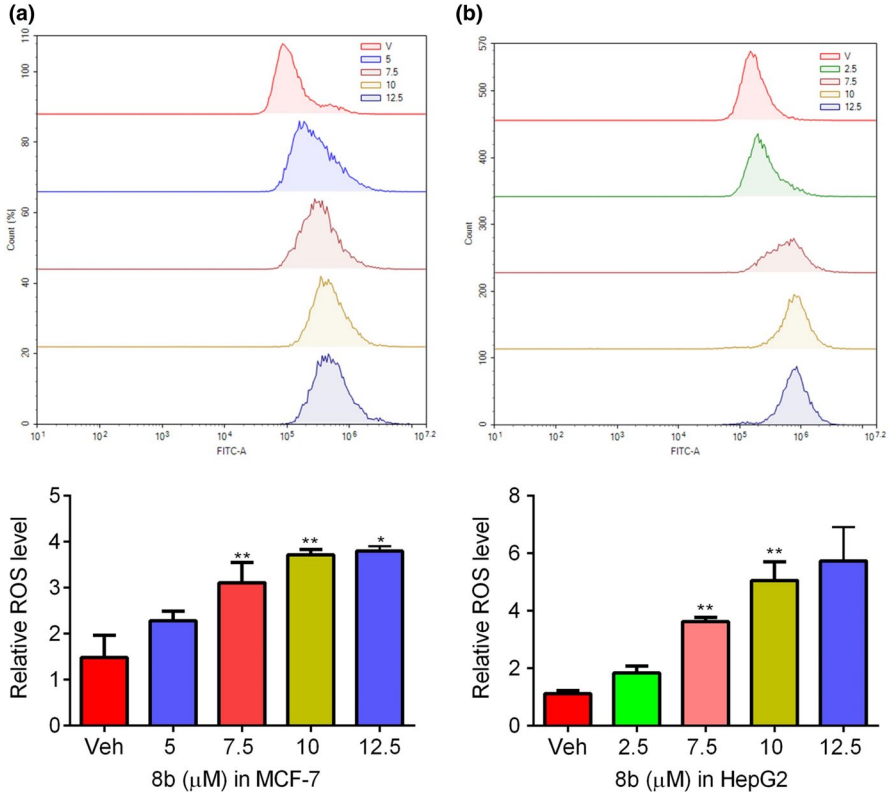

FIGURE 4 Compound **8b** induced the generation of ROS in cancer cells. (a) MCF-7 cell line was treated with compound **8b** at tested concentration for 24 hr, ROS accumulation was analyzed by flow cytometer; relative ROS level in MCF-7 was represented by a histogram. (b) HepG2 cell lines were treated with compound **8b** at tested concentration for 24 hr, ROS accumulation was analyzed by flow cytometer, and relative ROS level in HepG2 was represented by a histogram (*$p < .05$, **$p < .01$, compared to the vehicle group)

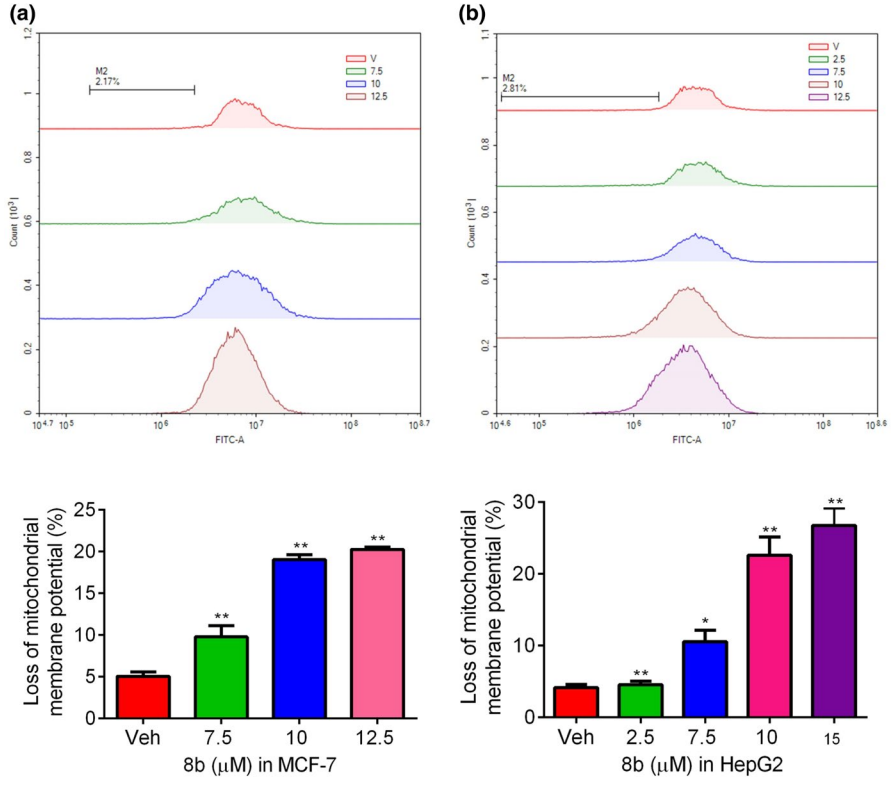

FIGURE 5 Compound **8b** caused the loss of mitochondrial membrane potential (Δψm). (a) MCF-7 cell was treated with compound **8b** at tested concentration for 24 hr, Δψm was analyzed by flow cytometer. The loss of mitochondrial membrane potential (%) was counted with histogram. (b) HepG2 cell were treated with compound **8b** at tested concentration for 24 hr; Δψm was analyzed by flow cytometer. The loss of mitochondrial membrane potential (%) was counted with histogram. (*$p < .05$, **$p < .01$, compared to the vehicle group)

potent compound in cell antiproliferation assay in four cancer cell lines. Further mechanism research proved that compound **8b** significantly induced the apoptosis in HCT116 cells, MCF-7 cells, MDA-MB-231 cells, and HepG2 cells. Meanwhile, G2/M-phase blocking was observed after treatment. Subsequently, we detected the ROS levels and Δψm of mitochondrial membrane potential and observed the uptrend and downtrend, respectively. Western blot assays and

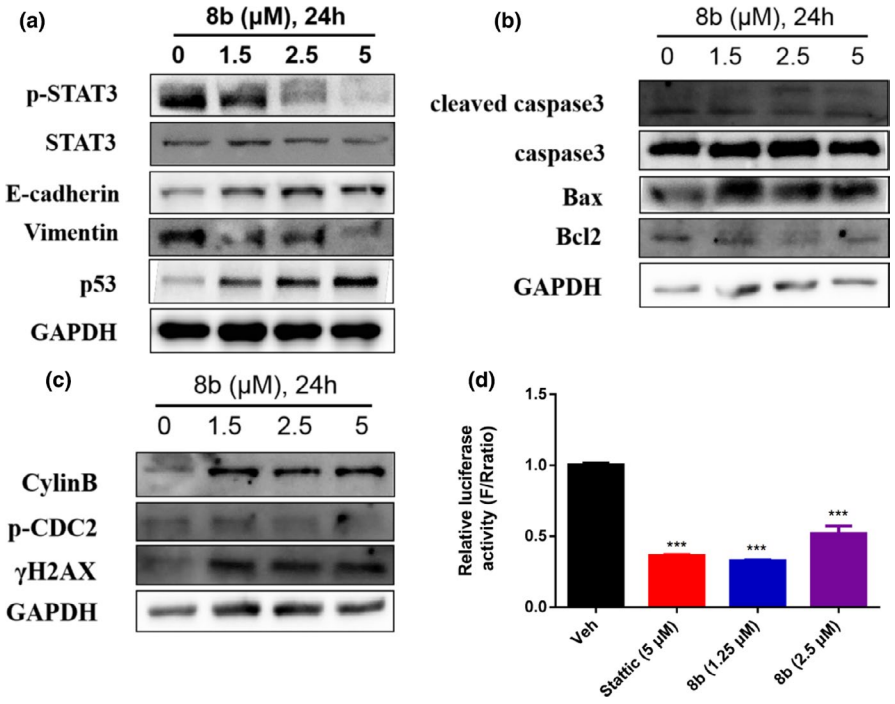

FIGURE 6 Western blot results of compound **8b**. (a) The protein level of STAT3, p-STAT3, E-cadherin, vimentin, p53 in HepG2 cells. (b) The protein level of cylin B, p-CDC2, γ2HAX in HepG2 cells. (c) The protein level of cleaved caspase 3, caspase 3, Bax, Bcl-2 in HepG2 cells. (d) HepG2 cells were transfected with pLuc-TK/STAT3 and pRL-TK before the treatment with **8b** for additional 48 hr; the results were expressed as relative luciferase activity (*$p < .05$, **$p < .01$, ***$p < .001$ compared to the vehicle group)

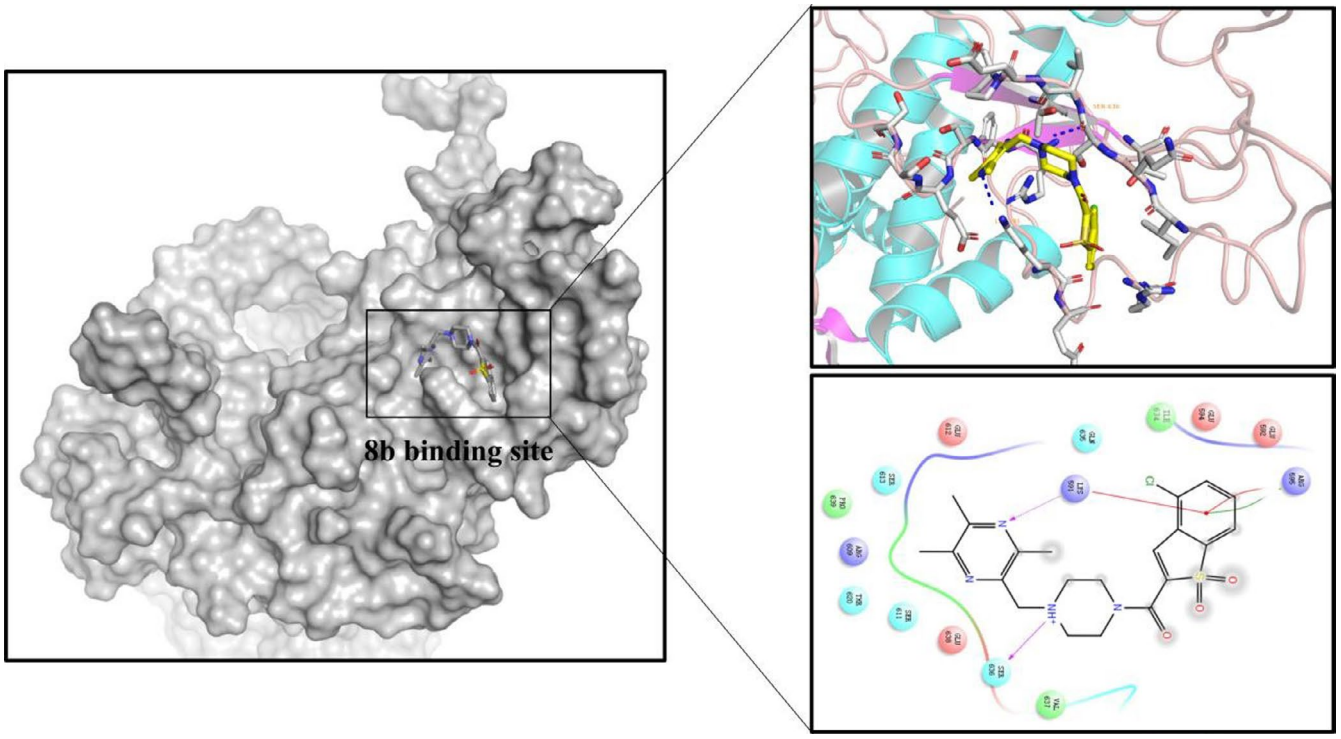

FIGURE 7 Molecular docking results. Predicted binding model of **8b** in STAT3 SH2 domain (PDB:1BG1), the figure was generated by using pymol

dual-luciferase reporter assays demonstrated that **8b** inhibited the phosphorylation of STAT3 and regulated the expression of proteins associated with apoptosis, cell cycle, and DNA damage. Docking study revealed that compound **8b** bound to pY and pY-X cavities of the STAT3 SH2 domain. In summary, all these evidences suggested compound **8b** a novel potent STAT3 inhibitor and a potential candidate for tumor treatment.

ACKNOWLEDGMENTS

We appreciate the Support Program of Science & Technology Department of Sichuan Provincial (no. 2021YFH0173).

CONFLICT OF INTEREST

The authors declare no conflict of interests.

DATA AVAILABILITY STATEMENT

The data that support the findings of this study are available from the corresponding author upon reasonable request.

REFERENCES

Barash, I. (2012). Stat5 in breast cancer: Potential oncogenic activity coincides with positive prognosis for the disease. *Carcinogenesis*, *33*(12), 2320–2325. https://doi.org/10.1093/carcin/bgs362

Benekli, M., Baumann, H., & Wetzler, M. (2009). Targeting signal transducer and activator of transcription signaling pathway in leukemias. *Journal of Clinical Oncology*, *27*(26), 4422–4432. https://doi.org/10.1200/JCO.2008.21.3264

Bhasin, D., Cisek, K., Pandharkar, T., Regan, N., Li, C., Pandit, B., Lin, J., & Li, P. K. (2008). Design, synthesis, and studies of small molecule STAT3 inhibitors. *Bioorganic & Medicinal Chemistry Letters*, *18*(1), 391–395. https://doi.org/10.1016/j.bmcl.2007.10.031

Bonnet, S., Archer, S. L., Allalunis-Turner, J., Haromy, A., Beaulieu, C., Thompson, R., Lee, C. T., Lopaschuk, G. D., Puttagunta, L., Bonnet, S., Harry, G., Hashimoto, K., Porter, C. J., Andrade, M. A., Thebaud, B., & Michelakis, E. D. (2007). A mitochondria-K+ channel axis is suppressed in cancer and its normalization promotes apoptosis and inhibits cancer growth. *Cancer Cell*, *11*(1), 37–51. https://doi.org/10.1016/j.ccr.2006.10.020

Bromberg, J., & Chen, X. (2001). STAT proteins: Signal tranducers and activators of transcription. *Methods in Enzymology*, *333*, 138–151. https://doi.org/10.1016/s0076-6879(01)33052-5

Casetti, L., Martin-Lanneree, S., Najjar, I., Plo, I., Auge, S., Roy, L., Chomel, J. C., Lauret, E., Turhan, A. G., & Dusanter-Fourt, I. (2013). Differential contributions of STAT5A and STAT5B to stress protection and tyrosine kinase inhibitor resistance of chronic myeloid leukemia stem/progenitor cells. *Cancer Research*, *73*(7), 2052–2058. https://doi.org/10.1158/0008-5472.CAN-12-3955

Chen, C. L., Loy, A., Cen, L., Chan, C., Hsieh, F. C., Cheng, G., Wu, B., Qualman, S. J., Kunisada, K., Yamauchi-Takihara, K., & Lin, J. (2007). Signal transducer and activator of transcription 3 is involved in cell growth and survival of human rhabdomyosarcoma and osteosarcoma cells. *BMC Cancer*, *7*, 111. https://doi.org/10.1186/1471-2407-7-111

Chen, H., Yang, Z., Ding, C., Chu, L., Zhang, Y., Terry, K., Liu, H., Shen, Q., & Zhou, J. (2013). Fragment-based drug design and identification of HJC0123, a novel orally bioavailable STAT3 inhibitor for cancer therapy. *European Journal of Medicinal Chemistry*, *62*, 498–507. https://doi.org/10.1016/j.ejmech.2013.01.023

Chen, H., Yang, Z., Ding, C., Xiong, A., Wild, C., Wang, L., Ye, N., Cai, G., Flores, R. M., Ding, Y., Shen, Q., & Zhou, J. (2014). Discovery of potent anticancer agent HJC0416, an orally bioavailable small molecule inhibitor of signal transducer and activator of transcription 3 (STAT3). *European Journal of Medicinal Chemistry*, *82*, 195–203. https://doi.org/10.1016/j.ejmech.2014.05.049

Chen, L. B. (1988). Mitochondrial membrane potential in living cells. *Annual Review of Cell Biology*, *4*, 155–181. https://doi.org/10.1146/annurev.cb.04.110188.001103

Chen, Y., Ruan, Z. X., Wang, F., Huangfu, D. S., Sun, P. H., Lin, J., & Chen, W. M. (2015). Novel oxazolidinone antibacterial analogues with a substituted ligustrazine C-ring unit. *Chemical Biology & Drug Design*, *86*(4), 682–690. https://doi.org/10.1111/cbdd.12537

Cohen-Kaplan, V., Jrbashyan, J., Yanir, Y., Naroditsky, I., Ben-Izhak, O., Ilan, N., Doweck, I., & Vlodavsky, I. (2012). Heparanase induces signal transducer and activator of transcription (STAT) protein phosphorylation: Preclinical and clinical significance in head and neck cancer. *Journal of Biological Chemistry*, *287*(9), 6668–6678. https://doi.org/10.1074/jbc.M111.271346

Darnell, J. J. (1997). STATs and gene regulation. *Science*, *277*(5332), 1630–1635. https://doi.org/10.1126/science.277.5332.1630

Furtek, S. L., Backos, D. S., Matheson, C. J., & Reigan, P. (2016). Strategies and approaches of targeting STAT3 for cancer treatment. *ACS Chemical Biology*, *11*(2), 308–318. https://doi.org/10.1021/acschembio.5b00945

Germain, D., & Frank, D. A. (2007). Targeting the cytoplasmic and nuclear functions of signal transducers and activators of transcription 3 for cancer therapy. *Clinical Cancer Research*, *13*(19), 5665–5669. https://doi.org/10.1158/1078-0432.CCR-06-2491

Han, J., Song, J., Li, X., Zhu, M., Guo, W., Xing, W., Zhao, R., He, X., Liu, X., Wang, S., Li, Y., Huang, H., & Xu, X. (2015). Ligustrazine suppresses the growth of HRPC cells through the inhibition of cap-dependent translation via both the mTOR and the MEK/ERK pathways. *Anti-Cancer Agents in Medicinal Chemistry*, *15*(6), 764–772. https://doi.org/10.2174/1871520615666150305112120

Hockenbery, D. M. (2002). A mitochondrial Achilles' heel in cancer? *Cancer Cell*, *2*(1), 1–2. https://doi.org/10.1016/s1535-6108(02)00087-9

Huang, M., Page, C., Reynolds, R. K., & Lin, J. (2000). Constitutive activation of stat 3 oncogene product in human ovarian carcinoma cells. *Gynecologic Oncology*, *79*(1), 67–73. https://doi.org/10.1006/gyno.2000.5931

Ji, P., Xu, X., Ma, S., Fan, J., Zhou, Q., Mao, X., & Qiao, C. (2015). Novel 2-carbonylbenzothiophene 1,1-dioxide derivatives as potent inhibitors of STAT3 signaling pathway. *ACS Medicinal Chemistry Letters*, *6*(9), 1010–1014. https://doi.org/10.1021/acsmedchemlett.5b00228

Kroemer, G., & Pouyssegur, J. (2008). Tumor cell metabolism: Cancer's Achilles' heel. *Cancer Cell*, *13*(6), 472–482. https://doi.org/10.1016/j.ccr.2008.05.005

Liao, Z., & Nevalainen, M. T. (2011). Targeting transcription factor Stat5a/b as a therapeutic strategy for prostate cancer. *American Journal of Translational Research*, *3*(2), 133–138.

Lin, L., Hutzen, B., Li, P. K., Ball, S., Zuo, M., DeAngelis, S., Foust, E., Sobo, M., Friedman, L., Bhasin, D., Cen, L., Li, C., & Lin, J. (2010). A novel small molecule, LLL12, inhibits STAT3 phosphorylation and activities and exhibits potent growth-suppressive activity in human cancer cells. *Neoplasia*, *12*(1), 39–50. https://doi.org/10.1593/neo.91196

Maritano, D., Sugrue, M. L., Tininini, S., Dewilde, S., Strobl, B., Fu, X., Murray-Tait, V., Chiarle, R., & Poli, V. (2004). The STAT3 isoforms alpha and beta have unique and specific functions. *Nature Immunology*, *5*(4), 401–409. https://doi.org/10.1038/ni1052

Park, I. H., & Li, C. (2011). Characterization of molecular recognition of STAT3 SH2 domain inhibitors through molecular simulation. *Journal of Molecular Recognition*, *24*(2), 254–265. https://doi.org/10.1002/jmr.1047

Ren, F., Geng, Y., Minami, T., Qiu, Y., Feng, Y., Liu, C., Zhao, J., Wang, Y., Fan, X., Wang, Y., Li, M., Li, J., & Chang, Z. (2015). Nuclear termination of STAT3 signaling through SIPAR (STAT3-interacting protein as a repressor)-dependent recruitment of T cell tyrosine phosphatase TC-PTP. *FEBS Letters*, *589*(15), 1890–1896. https://doi.org/10.1016/j.febslet.2015.05.031

Sanchez-Ceja, S. G., Reyes-Maldonado, E., Vazquez-Manriquez, M. E., Lopez-Luna, J. J., Belmont, A., & Gutierrez-Castellanos, S. (2006). Differential expression of STAT5 and Bcl-xL, and high expression of Neu and STAT3 in non-small-cell lung carcinoma. *Lung Cancer*, *54*(2), 163–168. https://doi.org/10.1016/j.lungcan.2006.07.012

Schust, J., Sperl, B., Hollis, A., Mayer, T. U., & Berg, T. (2006). Stattic: A small-molecule inhibitor of STAT3 activation and dimerization. *Chemistry & Biology*, *13*(11), 1235–1242. https://doi.org/10.1016/j.chembiol.2006.09.018

Song, H., Wang, R., Wang, S., & Lin, J. (2005). A low-molecular-weight compound discovered through virtual database screening inhibits Stat3 function in breast cancer cells. *Proceedings of the National Academy of Sciences USA*, *102*(13), 4700–4705. https://doi.org/10.1073/pnas.0409894102

Sun, Y., Yang, S., Sun, N., & Chen, J. (2014). Differential expression of STAT1 and p21 proteins predicts pancreatic cancer progression and prognosis. *Pancreas*, *43*(4), 619–623. https://doi.org/10.1097/MPA.0000000000000074

Wang, J., Hong, G., Li, G., Wang, W., & Liu, T. (2019). Novel homobivalent and polyvalent compounds based on ligustrazine and heterocyclic ring as anticancer agents. *Molecules*, *24*(24), 4505. https://doi.org/10.3390/molecules24244505

Wang, Y., Shen, Y., Wang, S., Shen, Q., & Zhou, X. (2018). The role of STAT3 in leading the crosstalk between human cancers and the immune system. *Cancer Letters*, *415*, 117–128. https://doi.org/10.1016/j.canlet.2017.12.003

Yamamoto, T., Sekine, Y., Kashima, K., Kubota, A., Sato, N., Aoki, N., & Matsuda, T. (2002). The nuclear isoform of protein-tyrosine phosphatase TC-PTP regulates interleukin-6-mediated signaling pathway through STAT3 dephosphorylation. *Biochemical and Biophysical Research Communications*, *297*(4), 811–817. https://doi.org/10.1016/s0006-291x(02)02291-x

Ye, Y., Zhang, T., Yuan, H., Li, D., Lou, H., & Fan, P. (2017). Mitochondria-targeted lupane triterpenoid derivatives and their selective apoptosis-inducing anticancer mechanisms. *Journal of Medicinal Chemistry*, *60*(14), 6353–6363. https://doi.org/10.1021/acs.jmedchem.7b00679

Yu, H., Pardoll, D., & Jove, R. (2009). STATs in cancer inflammation and immunity: A leading role for STAT3. *Nature Reviews Cancer*, *9*(11), 798–809. https://doi.org/10.1038/nrc2734

Yu, T., Qu, J., Wang, Y., & Jin, H. (2018). Ligustrazine protects chondrocyte against IL-1beta induced injury by regulation of SOX9/NF-kappaB signaling pathway. *Journal of Cellular Biochemistry*, *119*(9), 7419–7430. https://doi.org/10.1002/jcb.27051

Zhang, Y., Jin, Z., Zhou, H., Ou, X., Xu, Y., Li, H., Liu, C., & Li, B. (2016). Suppression of prostate cancer progression by cancer cell stemness inhibitor napabucasin. *Cancer Medicine*, *5*(6), 1251–1258. https://doi.org/10.1002/cam4.675

SUPPORTING INFORMATION

Additional supporting information may be found online in the Supporting Information section.

How to cite this article: Li, W.-Z., Xi, H.-Z., Wang, Y.-J., Ma, H.-B., Cheng, Z.-Q., Yang, Y., Wu, M.-L., Liu, T.-M., Yang, W., Wang, Q., Liao, M.-Y., Xia, Y., & Zhang, Y.-W. (2021). Design, synthesis, and biological evaluation of benzo[b]thiophene 1,1-dioxide derivatives as potent STAT3 inhibitors. *Chemical Biology & Drug Design*, 00, 1–15. https://doi.org/10.1111/cbdd.13939